Modal and non-modal stability of particle-laden channel flow

Joy Klinkenberg,[1,2] H. C. de Lange,[1] and Luca Brandt[2]

[1] *TU/e, Mechanical Engineering, 5600 MB, Eindhoven, The Netherlands*

[2] *Linné Flow Centre, KTH Mechanics, S-100 44 Stockholm, Sweden*

(Dated: April 18, 2011)

Abstract

Modal and non-modal linear stability analysis of channel flow with a dilute particle suspension is presented where particles are assumed to be solid, spherical and heavy. The two-way coupling between particle and fluid flow is therefore modeled by the Stokes drag only. The results are presented as function of the particle relaxation time and mass fraction. First, we consider exponentially growing perturbations and extend previous findings showing the potential for a significant increase of the critical Reynolds number. The largest stabilization is observed when the ratio between the particle relaxation time and the oscillation period of the wave is of order one. By examining the energy budget we show that this stabilization is due to the increase of the dissipation caused by the Stokes drag. The observed stabilization has led to the hypothesis that dusty flows can be more stable. However, transition to turbulence is most often subcritical in canonical shear flows where non-modal growth mechanisms are responsible for the initial growth of external disturbances. The non-modal analysis of the particle-laden flow, presented here for the first time, reveals that the transient energy growth is, surprisingly, increased by the presence of particles, in proportion to the particle mass fraction. The generation of streamwise streaks via the lift-up mechanism is still the dominant disturbance-growth mechanism in the particle laden flow: the length scales of the most dangerous disturbances are unaffected while the initial disturbance growth can be delayed. These results are explained in terms of a dimensionless parameter relating the particle relaxation time to the time scale of the instability. The presence of a dilute solid phase therefore may not always work as a flow-control strategy for maintaining the flow as laminar. Despite the stabilizing effect on modal instabilities, non-modal mechanisms are still strong in internal flows seeded with heavy particles. Our results indicate that the initial stages of transition in dilute suspensions of small particles are similar to the stages in a single phase flow.

I. INTRODUCTION

The dynamics of small inertial particles transported in a flow is crucial in many engineering and environmental applications. It is a long known fact that adding dust to a fluid may reduce the drag in pipe flows[1]. To explain this phenomenon it has been suggested that the dust delays transition and dampens the formation of turbulent structures. More recently, drag reduction has been demonstrated by direct numerical simulations in plane channel flow using heavy spherical particles[2], similarly to what has been observed with polymer or fibrous additives. Motivated by these results, we investigate whether the transition from laminar to turbulent flow might also be delayed, i.e. whether particles make the flow more stable. As a first step in this direction, the stability of a dusty-laminar flow is discussed in this paper.

The stability problem for a dusty gas was already formulated by Saffman in 1962[3]. He considered a plane parallel flow, where the base laminar profile is the same for the two phases considered, and an Eulerian description for the particle field; the coupling between fluid and solid phase is defined only through Stokes drag. In addition, a homogeneous distribution of particles is assumed and classic modal stability analysis performed. The particle perturbation velocities are expressed in terms of the fluid velocities and the stability problem reduces to solving a modified complex Orr-Sommerfeld equation. Saffman[3] distinguishes two different cases: fine and coarse dust. For fine dust, the particle relaxation time is small and the dust adjusts quickly to the gas flow. Therefore, the added particles only lead to an increase in density and consequently a decrease of the critical Reynolds number. Coarse dust, conversely, increases the critical Reynolds number and thus stabilizes the flow. In a later investigation, Michael[4] considers Poiseuille flow and presents neutral stability curves for several relaxation times. The results confirm that fine particles indeed decrease the critical Reynolds number whereas coarser particles increase it. Furthermore, Michael shows that very large/heavy particles have almost no effect on flow stability: the neutral stability curves retreats to the curve for the clean fluid when particles are too heavy to be affected by the fluid (ballistic limit).

The work by Michael[4] was extended by Rudyak *et. al.*[5] using an improved numerical accuracy. These authors[5] again considered the linear modal stability of plane Poiseuille flow seeded with small heavy particles. Besides the fact that they propose to change the dimensionless numbers to some having more relevant physical meaning, the general results stay the same: small particles decrease stability, while larger particles increase the stability of the flow. In this study, inhomogeneous particle concentration is also examined and it is shown that stability is modified, both enhanced and reduced, when increasing the particle concentration in two layers near the walls while keeping the total number of particles constant.

The stability of the flat-plate boundary-layer flow is studied by Asmolov and Manuilovich[6]. These authors adopt the same model as introduced by Saffman[3]; in this

case, however, the base flow differs from the case of single phase fluid in the presence of particles. For large particles and long relaxation times, the numerical analysis of Michael[4] becomes inaccurate, the neutral stability curves become irregular, and integration of the stability equation needs to be performed in the complex plane, as done also in Ref. 5. The dust suppresses the instability waves for a wide range of the particle size. The most efficient suppression takes place when the relaxation length of the particle velocity is close to the wavelength α of the Tollmien–Schlichting wave. The analysis in Ref. 6 is also extended to a polydisperse dust. The growth rate of disturbances does not differ much from the monodisperse dust, only discontinuities arise in the (α, R)-plane for damped disturbances (with R the Reynolds number). The number of discontinuities equals the number of different particle sizes present.

These investigations only used Stokes drag as coupling term between the two phases: however, more recent studies discuss also additional coupling terms, mostly in the context of turbulent flows, e.g. Ref. 7. The paper by Maxey and Riley[8] introduces the description of several forces arising between fluid and particles for different density ratios, namely the added mass term, a pressure gradient term, buoyancy and the Basset history term. The starting point of their analysis is the equation of motion proposed by Tchen[9] and modified by Corrsin and Lumley[10]. Boronin and Osiptsov[11] investigated the influence of the Saffman lift force[12] and a non-uniform particle distribution on the flow stability. The Saffman lift force itself has been investigated by several authors[13–15]. Furthermore the effect of the finite particle volume fraction is investigated by Vreman[16] and Boronin[17].

All investigations mentioned so far have considered only modal stability analysis. However, it is now understood that perturbation in wall-bounded shear flow can experience significant transient energy growth[18–21]; the latter is responsible for the initial linear amplification of external disturbances which lead to subcritical transition to turbulence. As example, the critical Reynolds number for channel flow is $R = 5772$, while experiments show transition at Reynolds numbers as low as $R \approx 1000$. From a mathematical point of view, this transient energy growth is related to the non-normality of the governing linear stability operator: non-orthogonal eigenfunctions can be linearly combined to yield a low energy initial condition. However, owing to the different decay rates, the initial cancellation is later lost and the perturbation energy increases before eventually decaying to zero in a stable system. From a physical point of view, transient growth is associated to the generation of elongated spanwise-periodic streamwise velocity perturbations. These streaks are induced by pairs of counter-rotating streamwise vortices via the so-called lift-up effect[22]. In such a context, modal stability analysis is only relevant to study the asymptotic behavior of the system at large times: non-modal input-output analysis is necessary to explore the possibility of transient energy growth. In this case, one wishes to know the largest possible energy amplification that can be obtained over a finite time. The initial condition leading to the largest possible growth is denoted *optimal disturbance* and it is indeed found to consist of streamwise vortices in shear flows. The growth of the streaks, induced by these streamwise

vortices, can be such that disturbances reach significant amplitudes and non-linear effects become important. In particular, it has been observed that streaks of high amplitude become susceptible to secondary inflectional instability leading to breakdown to turbulence.[23–25].

The aim of this paper is therefore to investigate for the first time the non-modal stability of particle-laden channel flows for different particle mass fraction and relaxation time. Although modal stability analysis shows a stabilization of the flow in the presence of particles, an effective delay of the turbulent onset in channel flows requires also damping of non-modal growth mechanisms.

II. GOVERNING EQUATIONS AND STABILITY ANALYSIS

A. Equations for particle-laden flows

We consider a channel flow seeded with solid spherical particles whose size is smaller than the characteristic scale of the flow. To perform our analysis, we adopt the continuous, or Eulerian, model introduced by Saffman[3]: the particles are assumed to be under the action of Stokes drag only; lift force, buoyancy and added mass are neglected. While the continuous approach is bound to fail in turbulent flows, owing to particle clustering and singularities in the particles field, it can still be retained valid for laminar flow and perturbation of it, such as in linear stability calculations[26]. In the following, p is the pressure, ρ the density of the fluid, N the number of particles per unit volume, r the radius of the particle and μ the dynamic viscosity. mN is the mass of the particles per volume with $m = \frac{4}{3}\pi r^3 \rho_p$ the mass of one particle, using the density of the particle ρ_p. Furthermore, K is the Stokes drag per relative velocity and defined as $K = 6\pi r\mu$. The governing equations for incompressible flow can be written as follows where u_i and u_{p_i} are the fluid and particle velocity respectively,

$$\rho\frac{\partial u_i}{\partial t} = -\frac{\partial p}{\partial x_i} - \rho u_j\frac{\partial u_i}{\partial x_j} + \mu\frac{\partial^2 u_i}{\partial x_j^2} + KN\left(u_{p_i} - u_i\right) \tag{1}$$

$$mN\frac{\partial u_{p_i}}{\partial t} = -mNu_{p_j}\frac{\partial u_{p_i}}{\partial x_j} + KN\left(u_i - u_{p_i}\right), \tag{2}$$

$$\frac{\partial N}{\partial t} = -\frac{\partial}{\partial x_i}\left(Nu_{p_i}\right) \tag{3}$$

$$\frac{\partial u_i}{\partial x_i} = 0. \tag{4}$$

The stability of this flow is investigated by considering a small perturbation u' to the base flow U. The base flow considered is Poiseuille flow driven by a constant pressure gradient. In the presence of a dispersed phase, the steady mean flow for both fluid and particles takes the form $U(y) = 1 - y^2$, $y \in [-1, 1]$, independent of the number of particles. Substituting $u = U + u'$, $u_p = U + u'_p$, $p = P + p'$ and $N = N_0 + N'$ in equations(1-4), linearized stability

equations are derived in a standard way[21]. These read (primes are omitted):

$$\frac{\partial u_i}{\partial t} = -\frac{\partial p}{\partial x_i} - U_j \frac{\partial u_i}{\partial x_j} - u_j \frac{\partial U_i}{\partial x_j} + \nu \frac{\partial^2 u_i}{\partial x_j^2} + \frac{K N_0}{\rho} \left(u_{p_i} - u_i\right) \tag{5}$$

$$\frac{\partial u_{p_i}}{\partial t} = -U_j \frac{\partial u_{p_i}}{\partial x_j} - u_{p_j} \frac{\partial U_i}{\partial x_j} + \frac{K}{m} \left(u_i - u_{p_i}\right) \tag{6}$$

$$\frac{\partial N}{\partial t} = -\frac{\partial}{\partial x_i} \left(NU + N_0 u_{p_i}\right) \tag{7}$$

$$\frac{\partial u_i}{\partial x_i} = 0. \tag{8}$$

The dimensional parameters used are reported in table I for clarity. Three non-dimensional parameters can be defined for this problem and they are given in table II where we follow the notation by Saffman[3]. They are the mass concentration f, defined as the mass of particles divided by the mass of the fluid per unit volume, the Reynolds number R, using channel half height L, and the Stokes number S defined as the particle relaxation time over the viscous time scale. Note however that S appears in the equations multiplied by R: SR can be seen as a Stokes number based on the convective time scale of the flow.

Table I: Physical parameters defining the particle laden flows under consideration.

N		m^{-3}	Number density of particles
K	$6\ \pi r \mu$	$\mathrm{kg\ s}^{-1}$	For sphere with radius r, constant
mN		$\mathrm{kg\ m}^{-3}$	Mass of dust per unit volume
s	$\frac{KN_0}{\rho_f}$	s^{-1}	Constant, dimension of frequency
τ	$\frac{m}{K} = \frac{f}{s} (= \frac{2}{9} \frac{r^2}{\nu} \frac{\rho_p}{\rho_f})$	s	Relaxation time

Table II: Definition of the non-dimensional numbers used.

f	$\frac{m_p}{m_f}$	-	Mass concentration
R	$\frac{\rho U L}{\mu}$	-	Reynolds Number
S	$\frac{\nu \tau}{L^2} = \frac{2}{9} \frac{r^2}{L^2} \frac{\rho_p}{\rho_f}$	-	Dimensionless relaxation time

For the particular configuration considered, the equation for the particle distribution N_0 (equation 7) is decoupled from the rest of the system. As a consequence, Squire's theorem can be extended to this case and a complex Orr-Sommerfeld equation can be derived for the

stability of the flow[3,4], which has been considered in the past. However, we are also interested in the non-modal stability of the full three-dimensional problem and introduce therefore the initial value problem for the particle velocities and for the wall-normal velocity v and wall-normal vorticity $\eta = \frac{\partial u}{\partial z} - \frac{\partial w}{\partial x}$ of the fluid, analogous to the standard Orr-Sommerfeld-Squire system used for parallel single phase flows. The corresponding system of linearized equations in dimensionless form is given by:

$$\begin{aligned}
-\frac{\partial}{\partial t}\nabla^2 v &= \left[\left(U\frac{\partial}{\partial x} + \frac{f}{SR}\right)\nabla^2 - U''\frac{\partial}{\partial x} - \frac{1}{R}\nabla^4\right] v + \\
&\quad + \frac{f}{SR}\left(\frac{\partial^2 u_p}{\partial x \partial y} + \frac{\partial^2 w_p}{\partial y \partial z} - \frac{\partial^2 v_p}{\partial x^2} - \frac{\partial^2 v_p}{\partial z^2}\right) \qquad (9)\\
\frac{\partial \eta}{\partial t} &= \left[-U\frac{\partial}{\partial x} + \frac{1}{R}\nabla^2 - \frac{f}{SR}\right]\eta + \frac{f}{SR}\left(\frac{\partial u_p}{\partial z} - \frac{\partial w_p}{\partial x}\right) - \frac{\partial v}{\partial z}U' \qquad (10)\\
\frac{\partial u_p}{\partial t} &= -U\frac{\partial u_p}{\partial x} - v_p\frac{\partial U}{\partial y} + \frac{1}{SR}(u - u_p) \qquad (11)\\
\frac{\partial v_p}{\partial t} &= -U\frac{\partial v_p}{\partial x} + \frac{1}{SR}(v - v_p) \qquad (12)\\
\frac{\partial w_p}{\partial t} &= -U\frac{\partial w_p}{\partial x} + \frac{1}{SR}(w - w_p) \qquad (13)
\end{aligned}$$

The boundary conditions of this system are $v = \eta = u_p = v_p = w_p = 0$ at both walls.

In the limit of $SR \to 0$, Lagrangian limit ($r \ll L$), the coupling between the fluid and particle motion is very strong and particles behave as passive tracers. The particles have a very small relaxation time and will adjust to the fluid almost immediately. This results in an effective increase in density of the total flow, for which a modified Reynolds number R_m can be defined:

$$R_m = \frac{(1+f)\,\rho U L}{\mu}.$$

In the limit $SR \to \infty$, ballistic limit ($\rho_p \ll \rho_f$), the equation describing the particles motion is decoupled from the particle velocity. Particles are too heavy to be affected by the fluid and perturbations in the particle velocity are simply advected by the base flow.

B. Modal Stability

To study modal linear stability, we assume wave-like perturbations

$$q = \hat{q}(y)e^{i(\alpha x + \beta z - \omega t)},$$

with $q = (v, \eta, u_p, v_p, w_p)^T$. In the expression above, α and β define the streamwise and spanwise wavenumber of the perturbation, respectively, while ω is a complex frequency: $\Im(\omega) > 0$ indicates solutions exponentially growing in time. Here we will mainly focus on the

onset of the instability, $\Im(\omega)$ equals zero, and report neutral stability curves. As mentioned above, the neutral stability curve can be computed assuming two-dimensional perturbations since a modified version of Squire's theorem holds for the complex Orr-Sommerfeld equation[3] derived from equations (9, 11, 12).

C. Non-modal Stability

As discussed in the introduction, when the eigenvectors of the system are non-orthogonal, transient growth is possible even in asymptotically stable systems. Input-output or non-modal analysis is then necessary. The aim of such analysis is to determine the largest possible growth that can be achieved during a finite time interval; this is called optimal growth. The initial condition yielding optimal growth is denoted as optimal initial condition. If we indicate the discretized governing linear equations (9-13) in compact form as

$$\frac{\partial q}{\partial t} = Lq, \tag{14}$$

the largest possible energy growth at time t is the norm of the evolution operator, or propagator, $\mathcal{T} = \exp(tL)$. To quantify the energy growth, we use the kinetic energy of the full system defined as the kinetic energy of the fluid and of the particles

$$E_{kin} = \frac{1}{2}\left(m_f u_i^2 + m_p u_{p_i}^2\right), \tag{15}$$

with m_f and m_p the mass of the fluid and the particles respectively.
A matrix M can be associated with the energy norm. This is applied directly to the vector $q = [v, \eta, u_p, v_p, w_p]^T$ to give the kinetic energy integrated over the volume V

$$E(t) = \frac{1}{2}\int_V q^H M q dV. \tag{16}$$

In this study, we are not only interested in optimizing the total energy of the system. We wish also to investigate the optimal way to excite a response in the fluid/particles by an initial condition consisting only of perturbations in the fluid/particle velocity. To this aim we introduce the input disturbance q_{in}, the output q_{out} and corresponding input and output operators B and C. The input q_{in} consists of those quantities we wish to optimize for at time $t = 0$, while q_{out} defines the quantities we want to have amplified at time t. The dynamics of the system is still described by (14); to restrict the initial condition to q_{in} we need to define the input operator B such that $q = Bq_{in}$. In analogy, to study only the response q_{out}, C is defined such that $q_{out} = Cq$. The evolution operator from $q_{in}(t = 0)$ to $q_{out}(t)$ becomes therefore

$$\mathcal{T} = C\exp(tL)B. \tag{17}$$

Finally we define the input and output energy matrix with $M_{in} = F_{in}F_{in}^H$ and $M_{out} = F_{out}F_{out}^H$ and the corresponding norms as $||q_{in}||_{E_{in}} = ||F_{in}q_{in}||_2$, $||q_{out}||_{E_{out}} = ||F_{out}q_{out}||_2$.

Using the definition for optimal growth[21] one can show that the optimal growth corresponds to the 2-norm of the matrix

$$\begin{aligned} G(t) &= \frac{||q_{out}(t)||_{E_{out}}}{||q_{in}(0)||_{E_{in}}} = \frac{||\mathcal{T}q_{in}(0)||_{E_{out}}}{||q_{in}(0)||_{E_{in}}} = \frac{||F_{out}\mathcal{T}q_{in}(0)||_2}{||F_{in}q_{in}(0)||_2} = \\ &= \frac{||F_{out}\mathcal{T}F_{in}^{-1}F_{in}q_{in}(0)||_2}{||F_{in}q_{in}(0)||_2} = ||F_{out}\mathcal{T}F_{in}^{-1}||_2 = ||F_{out}C\exp(tL)BF_{in}^{-1}||_2. \end{aligned} \tag{18}$$

The classic computation of the optimal growth is retrieved when $F_{in} = F_{out}$ and $C = B = I$.

D. Energy analysis

An equation for the evolution of the kinetic energy of the system can be derived by multiplying equation (5) with u_i and equation (6) by u_{p_i}. Adding the two energies using a factor f to account for the particle mass and integrating over the total volume of the system V gives

$$\frac{\partial E_v}{\partial t} = -\int_V u_i u_j \frac{\partial U_i}{\partial x_j} dV - \frac{1}{Re}\int_V \frac{\partial u_i}{\partial x_j}\frac{\partial u_i}{\partial x_j} dV - f\int_V u_{p_i}u_{p_j}\frac{\partial U_i}{\partial x_j} dV - \frac{f}{SR}\int_V (u_i - u_{p_i})^2\, dV \tag{19}$$

where the divergence terms disappear owing to periodic boundary conditions and zero velocity at the walls.

The first two terms in (19) represent production of kinetic energy of the perturbation due to the work of the Reynolds stress $u_i u_j$ against the shear of the base flow and viscous dissipation in the fluid. The third term, appearing in the presence of particles, accounts for the production of particle kinetic energy against the mean shear of the particle base motion. The last term accounts for fluid/particle interactions and it is always negative. The fluid-particle interaction always introduces a loss in energy. One can therefore expect that, as a results of the optimization, particles and fluid will tend to have the same velocity in order to reduce losses. When $u_{p_i} = u_i$ the dissipative term equals zero and the production of kinetic energy is enhanced by the presence of the particles, by a factor proportional to their mass fraction. When examining the energy gain of particles only,

$$\frac{\partial E_{v_p}}{\partial t} = -f\int_V u_{p_i}u_{p_j}\frac{\partial U_i}{\partial x_j} dV + \frac{f}{SR}\int_V (u_i u_{pi} - u_{p_i}u_{p_i})\, dV, \tag{20}$$

we see that when $SR \to \infty$, the coupling between the particle and fluid velocities becomes negligible and the last term in equation (20) vanishes. This results in a particle energy equation without dissipation, which then can result in unbounded growth of the particle energy, the inviscid Orr-Mechanism[27].

The production and dissipation terms in equation (19) can be computed separately to gain insight into the instability mechanisms.[28] Assuming normal mode expansion, $(E, D, D_s, T_y, T_{p_y}) = (\hat{E}, \hat{D}, \hat{D}_s, \hat{T}_y, \hat{T}_{p_y})e^{2\omega_i t}$, with T_y and T_{p_y} the energy production terms, D the viscous dissipation, D_s the losses induced by the coupling Stokes drag and E the total perturbation kinetic energy. These terms become of the form (in 2 dimensions)

$$\hat{E} = \int_{-1}^{1} (\hat{u}\hat{u}^* + \hat{v}\hat{v}^*)\, dy \tag{21}$$

$$\hat{T}_y = \int_{-1}^{1} -(\hat{u}\hat{v}^* + \hat{u}^*\hat{v})\frac{dU}{dy}dy \qquad \hat{T}_{p_y} = \int_{-1}^{1} -(\hat{u_p}\hat{v_p}^* + \hat{u_p}^*\hat{v_p})\frac{dU}{dy}dy \tag{22}$$

$$\hat{D} = \int_{-1}^{1} 2\left(\frac{\partial \hat{u}_i}{\partial x_j} \cdot \frac{\partial \hat{u}_i}{\partial x_j}^*\right) dy \qquad \hat{D}_s = \int_{-1}^{1} ((\hat{u}_i - \hat{u}_{p_i})(\hat{u}_i - \hat{u}_{p_i})^*)\, dy, \tag{23}$$

where * indicates the complex conjugate.
Using equation (20) one can show that

$$\omega_i = \frac{\hat{T}_y}{2\hat{E}} + \frac{\hat{T}_{p_y}}{2\hat{E}} - \frac{\hat{D}}{2\hat{E}} - \frac{\hat{D}_s}{2\hat{E}}. \tag{24}$$

The different terms in this equation can be evaluated using the eigenvector from the stability analysis $(\hat{u}, \hat{v}, \hat{u}_p, \hat{v}_p)$.Variation of the production terms and of the Stokes drag is used to understand how modal stability is affected by the presence of particles. Note that the different terms should add to the growth rate ω_i, the imaginary part of the eigenmode. Eq. (24) therefore represents an a posteriori validation of the numerics.

E. Numerical method

Discretization of the equations is done using a Chebyshev collocation method in y-direction[23]. For most of the computations presented we used $n_y = 37$, with n_y being the number of collocations points. Tests were performed with $n_y = 67, 167$ to validate the accuracy of the results.

For the computation of the neutral stability, integration in the complex $y-$plane is performed to remove singularity in the limit of $SR \to \infty$[5,6]. To validate our implementation we report in Figure 1 a comparison with the results of Rudyak *et. al.*[5].

For the computation of transient growth, the energy matrix M is built to compute the

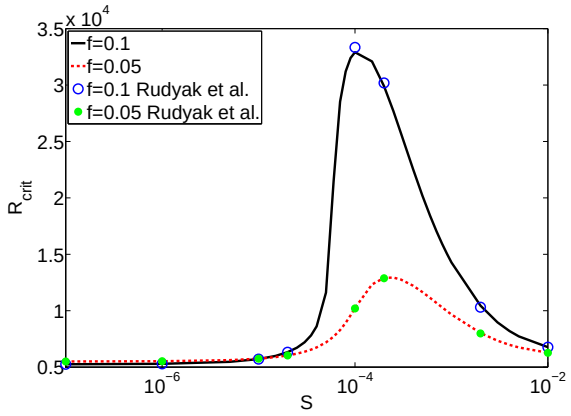

Figure 1: The critical Reynolds number as a function of dimensionless relaxation time S. A comparison between the present results and those in Ref. 5

kinetic energy of the fluid and particles

$$M = \begin{pmatrix} \left(-\frac{D^2}{k^2}+1\right) I_w & 0 & 0 & 0 & 0 \\ 0 & \frac{1}{k^2} I_w & 0 & 0 & 0 \\ 0 & 0 & f I_w & 0 & 0 \\ 0 & 0 & 0 & f I_w & 0 \\ 0 & 0 & 0 & 0 & f I_w \end{pmatrix}, \tag{25}$$

where I_w is a diagonal matrix performing spectral integration in y direction. As M is diagonal, this can be easily factorized $M = U\Sigma U^H$ using Singular Value Decomposition (SVD). This can be done for M_{in} as well as M_{out} to define F_{in}, F_{in}^{-1},F_{out} and F_{out}^{-1}: given $M = U\Sigma U^H$, $F = U\Sigma^{1/2}$.

III. RESULTS

A. Modal analysis

Considering the least stable eigenvalue of our system of equations, the neutral stability curves for different values of S are given in figure 2. The critical Reynolds number is seen to decrease for small $S(S = 1 \cdot 10^{-7})$, to increase for intermediate S, while for larger S it returns to the value found in Poiseuille flow without particles.

When S is very small, the particles are very small and just follow the fluid: relaxation time is fast and the particles adjust almost immediately to the fluid velocity. Therefore, the particles just act as to increase the total density of the system, thus lowering the critical Reynolds number by a factor $(1 + f)$. The neutral stability curves would coincide when instead of R, the Reynolds number of the mixture, R_m, is taken into account. For large

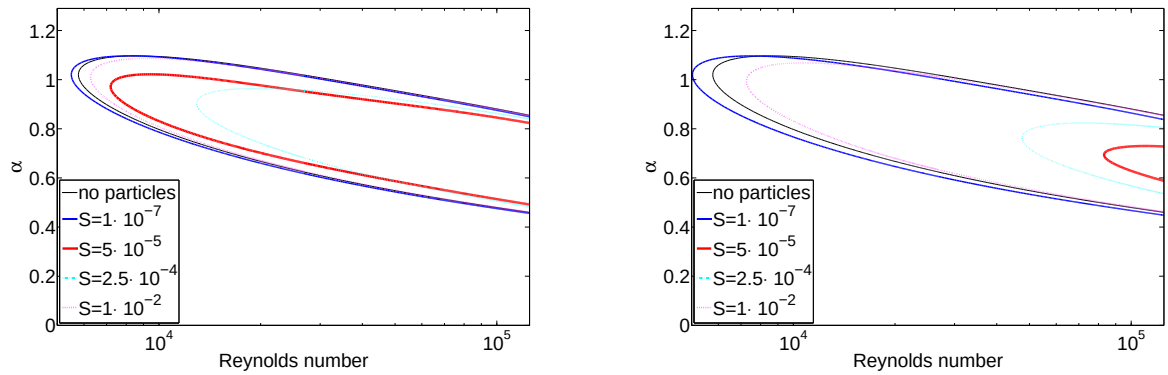

(a) $f = 0.05$ (b) $f = 0.15$

Figure 2: (Color online) Neutral stability curves for a particle laden flow with $S = [1 \cdot 10^{-7}, 5 \cdot 10^{-5}, 2.5 \cdot 10^{-4}, 1 \cdot 10^{-2}]$ and $f = 0.05$ (a), $f = 0.15$ (b). As reference, also the curve for a single phase flow is given.

values of S, however, the heavy and large particles are not able to interact with the fluid, thus they have no effect on the flow stability. In between these two extremes, the particles do interact with the flow and they have a positive effect on the flow stability; the critical Reynolds number increases with respect to the single phase channel flow. On the other hand, both the wavenumber and the phase velocity corresponding to the critical Reynolds number decreases. Our results are in agreement with the results in Ref. 3–5, obtained using the complex Orr-Sommerfeld equation.

It can be noted that the mass fraction f affects the value of the critical Reynolds number: more particles have larger stabilizing effect. For mass fraction $f = 0.15$, R_{crit} can grow to as much as 10^5, i.e. almost two order of magnitude. When increasing f, a second effect is that the value of S yielding the largest critical Reynolds number decreases.

In figure 3 we display the critical Reynolds number versus $St_\omega = SR\omega_r$; this is the ratio of the particle relaxation time to the period of the wave and can be interpreted as stability Stokes number. With this scaling, the largest reduction of the growth rate is observed for $St_\omega = \mathcal{O}(1)$ for all values of the mass fraction f. In other words, particles have a stabilizing effect on the flow when their relaxation time is close to the pulsation of the least stable waves.

To better understand this behavior, we consider the energy budget given in equation (19), where the expressions in (21-23) are used to compute the production and dissipation terms. Table III shows the results of these computations using $R = 1.25 \cdot 10^4$, $\alpha = 1$, $f = [0\ 0.05]$ and $SR = [0.001\ 1\ 5\ 10\ 100]$ In the last column we report the difference between the system eigenvalue and the growth rate estimated by the energy balance as further validation of our implementation. Figure 4 shows the production and dissipation terms versus the particle

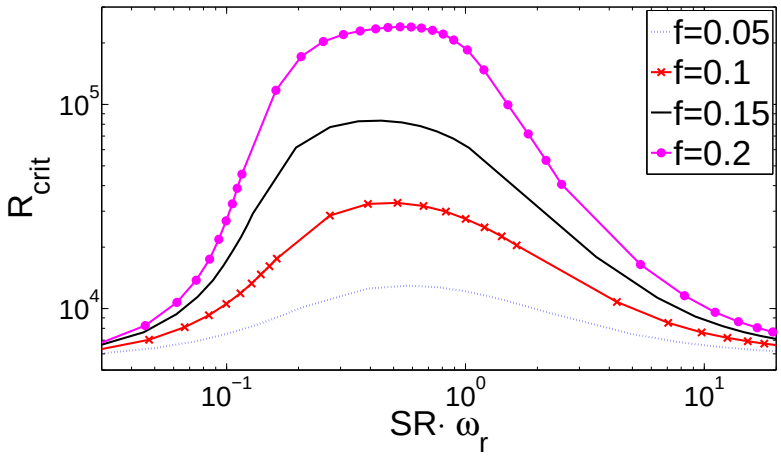

Figure 3: (Color online) Critical Reynolds number as a function of $St_\omega = SR\omega_r$ for $f = [0.05, 0.1, 0.15, 0.2]$, where $SR\omega_r$ is the ratio of the particle relaxation time to the period of the wave. The larger the f, the larger the critical Reynolds number R_{crit}.

relaxation time SR. It can be noted that the total energy production, $\hat{T}_y + \hat{T}_{y_p}$, and the viscous dissipation are almost constant with SR. The energy losses induced by the Stokes drag are initially very low but increase significantly when $SR \approx 1$. The large increase of $\hat{D}_s$ is therefore responsible for the stabilization documented above.

SR	f	$\frac{\hat{T}y}{2\hat{E}} \cdot 10^3$	$\frac{\hat{T}py}{2\hat{E}} \cdot 10^3$	$\frac{\hat{D}}{2\hat{E}} \cdot 10^3$	$\frac{\hat{D}s}{2\hat{E}} \cdot 10^3$	$\Sigma(\hat{T} - \hat{D}) \cdot 10^3$	$\omega_i \cdot 10^3$	Δ_ϵ
-	0	9.9442	0	5.7273	0	4.2169	4.2046	0.0123
0.001	0.05	9.4227	0.4790	5.6611	0.0074	4.2331	4.2206	0.0125
1	0.05	4.7140	5.7205	5.5637	5.5503	-0.6794	-0.6915	0.0121
5	0.05	5.9511	4.9145	5.4490	6.7058	-1.2892	-1.3006	0.0114
10	0.05	7.6115	3.9600	5.4401	5.7641	0.3673	0.3558	0.0115
100	0.05	8.5340	1.6584	5.0170	1.6262	3.5492	3.5382	0.0110

Table III: Production and dissipation terms for modal stability with $\alpha = 1$ and $R = 1.25 \cdot 10^4$. Production terms T_y and T_{p_y} are positive, while D and D_s are negative. The difference Δ_ϵ between the computed eigenvalue and the growth rate estimated by the energy budget is reported in the right-most column.

Finally, the eigenfunctions of the most unstable mode for $\alpha = 1$ and Reynolds number 10^4 are given in figure 5, both for a clean fluid and for a particle-laden flow. The single phase fluid has an unstable mode, while the particle laden flow with $f = 0.15$ is stable. The streamwise u- and wall-normal v-velocities, depicted in figure 5(a) are similar for single phase and particle laden flow. For particle laden flow, the maximum u-velocity is larger for

the same kinetic energy of the disturbance, although this value is reached further away from the walls. The fluid and particle velocities for the case of particle laden flow are shown in figure 5(b). The disturbance particle velocity u_p is larger than that of the fluid, while the wall-normal particle velocity, v_p, is smaller. The difference in the u_i and u_{p_i} velocities are responsible for the increase of the critical Reynolds number, as the difference between these values stabilizes the flow by introducing extra dissipation in the system (cf. equation 19).

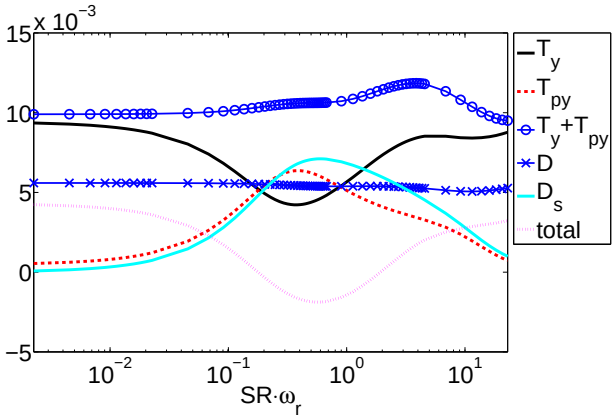

Figure 4: (Color online) Energy as a function of $St_\omega = SR\omega_r$ for $f = 0.05$, $R = 12500$ and $\alpha = 1$. The total production is also shown.

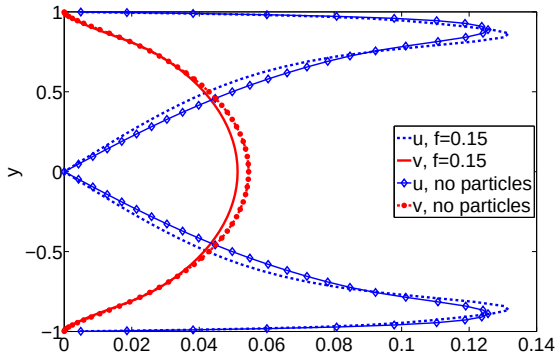

(a) u, v for $f = [0\ 0.15]$

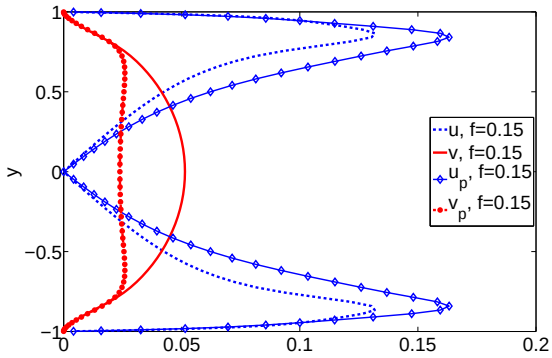

(b) u, u_p, v and v_p for $f = 0.15$

Figure 5: (Color online) Eigenfunctions at $R = 10^4$, $\alpha = 1$, using $S = 2.5 \cdot 10^{-4}$ and particle concentration $f = 0.15$. (a) shows the absolute velocities u and v for flow with and without particles. (b) shows absolute particle and fluid velocities for a particle laden flow.

B. Non-modal analysis

As discussed earlier, non-modal growth mechanisms are responsible for sub-critical transition to turbulence in shear flows. We wish to investigate, therefore, whether these are affected by the presence of the particles in the same way as the linear modal stability. This would imply that particles may induce significant transition delay. First, we introduce the quantities that will be considered in the following. The transient growth for a perturbation with wavenumbers $(\alpha, \beta) = (0, 2)$ in a single phase flow with $R = 2000$ is given in figure 6. In this example, pertaining to the wavenumber pair yielding the largest amplification in Poiseuille flow, the optimal growth is given as a function of time, as defined in equation (18). The curve is the envelope of the amplification curves of all initial conditions, in other words the maximum response to each optimal initial condition $q_0(t; Re, \alpha, \beta, f, S)$ is used to define this curve. The maximum growth, G_{max}, presented in figure 6, is an interesting parameter to be used to investigate the influence of particles on fluid flow as this is the global maximum in time of possible energy growth,

$$G_{max} = \max_t G(t) .$$

Preliminary calculations indicate that, in agreement to the case without particles, the largest non-modal amplification is attained by streamwise independent perturbations, where $\alpha = 0$. Therefore, in the following, we will present results of the non-modal analyses as curves of G_{max} versus α or β in which β and α are in turn set to zero. The case $\beta = 0$ will also be considered, in analogy to previous investigations in single phase shear flows[29], to examine the effect of particles on the Orr-mechanism and the optimal triggering of modal disturbances.

As already mentioned, results for nine different cases will be presented. In addition to these, results for the single phase flow, or reference flow, will also be displayed in each plot. All these cases are given in figure 7 for $S = 5 \cdot 10^{-5}$, $R = 2000$ and $f = 0.15$. Results are reported both for spanwise waves, $\alpha = 0$ in 7(a-b), and streamwise waves, $\beta = 0$ in 7(c-d). The cases displayed are denoted as $initial \rightarrow final$ with reference to the quantities used in the definitions of input and output energy norms; when both the particle and fluid kinetic energy are considered in the input/output norm, the case is denoted as *all*.

Comparing the results for streamwise (α) and spanwise (β) perturbations, it is obvious that spanwise perturbations lead to higher energy gain than streamwise perturbations. This result is in agreement to results of single phase flow, as already presented in Ref. 30–32. The spanwise perturbations consist of counter-rotating streamwise vortices, which induce high- and low-speed streaks owing to the lift-up effect.

1. *Spanwise-dependent disturbances*

The results for streamwise-independent spanwise-periodic disturbances are first discussed referring to the results shown in figure 7(a-b). The energy gain for the case $all \rightarrow all$ provides

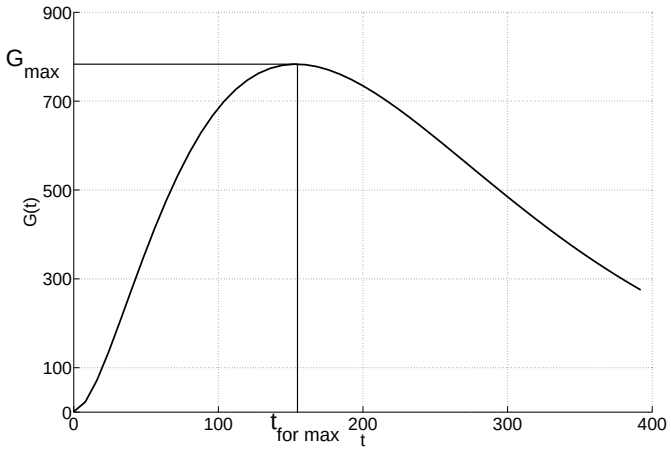

Figure 6: Transient growth for (α, β)=(0,2) and $R = 2000$ for a clean fluid. G_{max} indicates the largest growth in energy while $t_{for\ max}$ indicates the time needed to reach this maximum

the largest possible energy growth, the amplification is augmented by a factor $(1 + f)^2$ with respect to the flow without particles. The optimal energy growth for the total system is thus larger for particle-laden flows. The optimal gain in the case of a non-zero initial fluid velocity only ($fluid \rightarrow all$) also gives response larger than that in the clean flow, which may be expected since the particles contribute to the final energy as well. The growth is however smaller than for $all \rightarrow all$. The level of perturbation induced by perturbations in the particle motion, induced by stirring the particles with some external force, $part \rightarrow all$, is much lower in comparison to the previous cases; this indicates that initial particle disturbances are less effective to excite the flow. This can be explained by the low mass fraction of the solid phase in our model.

Considering the final particle velocity only ($initial \rightarrow part$) indicates the possibility to induce mixing in the density distribution. The values of the possible energy amplification are small, about $1/f$ lower than for the fluid velocity. However, the particle velocity is the same as the fluid velocity, and the gain is small only because the mass fraction is small, $f = 0.15$. The cases $all \rightarrow part$ and $fluid \rightarrow part$ are close to each other, suggesting a small amplification $part \rightarrow part$, which is indeed the case.

The final three cases examined deal with the optimal growth of the fluid flow perturbations (figure 7b). The fluid is able to gain more energy from the system when particles are present, compare $all \rightarrow fluid$ to no-particles. The fluid, however, is not able to gain much energy from the particles only ($part \rightarrow fluid$), while the $fluid \rightarrow fluid$ case is very close to the single phase optimal growth. This may indicate that losses due to the particle-fluid interactions are weak for the parameters in figure 7. As shown below, however, we observe a

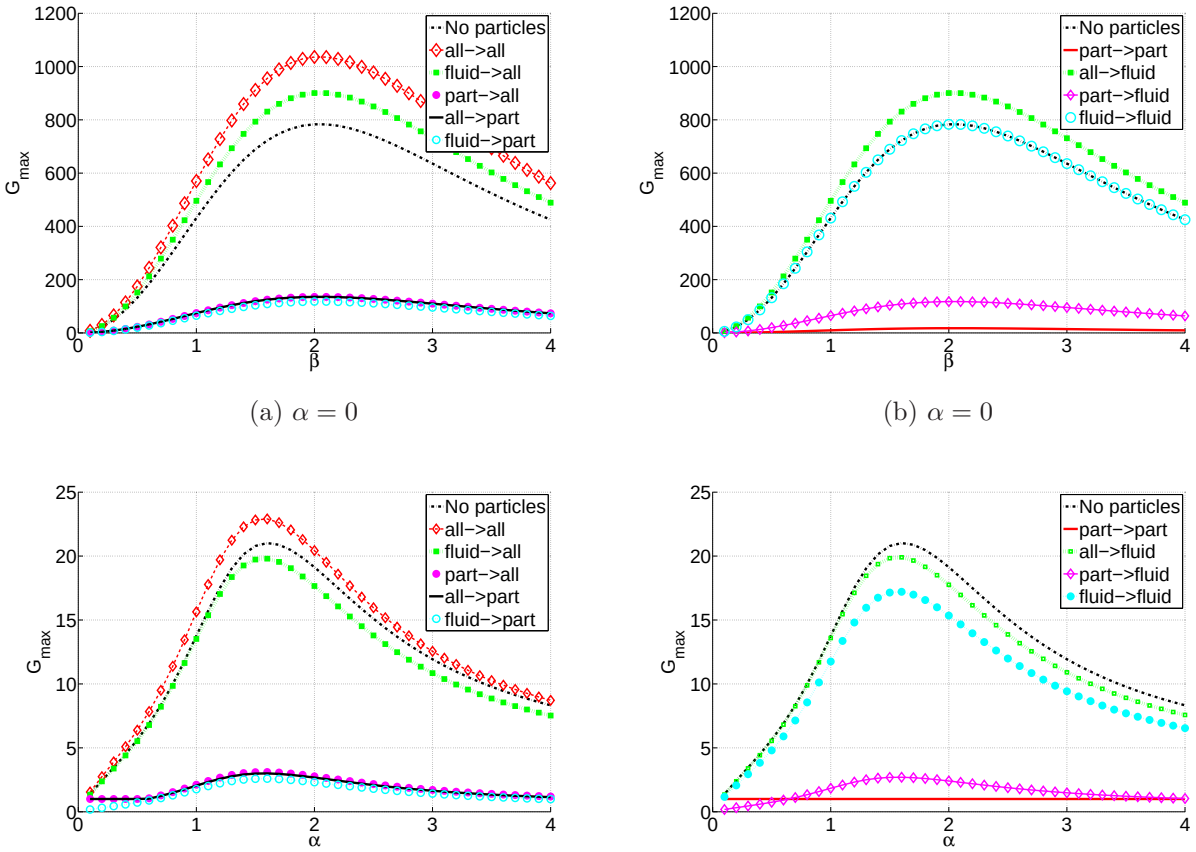

(a) $\alpha = 0$ (b) $\alpha = 0$

(c) $\beta = 0$ (d) $\beta = 0$

Figure 7: (Color online) Optimal growth for all 9 cases using $S = 5 \cdot 10^{-5}$, $R = 2000$ and $f = 0.15$, for spanwise (top) and streamwise (bottom) disturbances. As reference, also the single phase optimal growth is displayed. For clarity, the nine cases are divided into two figures (left and right).

more complicated interplay between initial losses induced by interaction with the particles and the larger amplification observed in the case $all \rightarrow fluid$.

As seen above when considering the total energy of the system (equation 19), the dissipation of energy due to fluid/particle interactions vanishes when the fluid and particle velocity are equal. It is therefore not surprising that the optimal initial condition has the same velocity for fluid and particles in the case $all \rightarrow all$. For the values of S allowed by our model, moderate SR, also in the case of zero initial particle velocity, the difference (and thus the Stokes drag) becomes small and eventually zero for relatively long optimization intervals. In figure 8 we report the optimal initial condition (a) and the optimal response (b) for the case $fluid \rightarrow fluid$ with $\beta = 2, S = 5 \cdot 10^{-5}, f = 0.15$ and $R = 5000$. The initial condition consists of a pair of counter-rotating streamwise vortices spanning the full channel

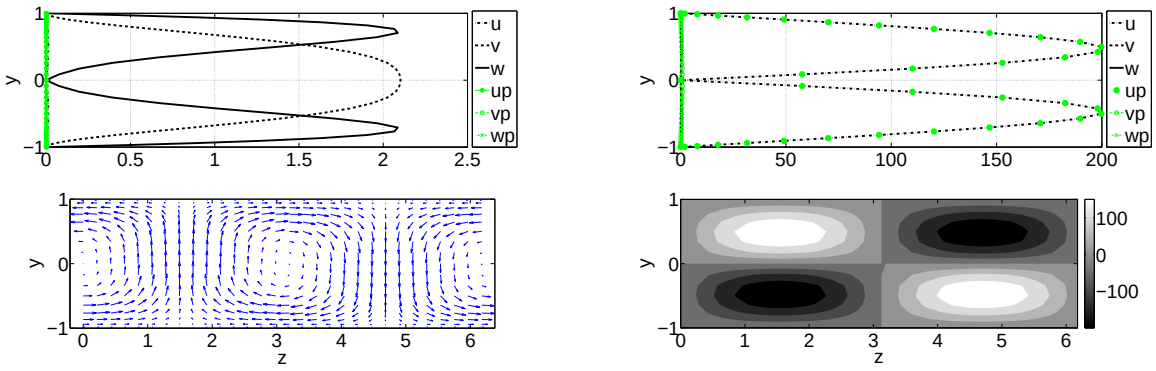

(a) Initial condition

(b) Response

Figure 8: (Color online) Optimal initial condition and response for the case $fluid \rightarrow fluid$ with $\beta = 2, S = 5 \cdot 10^{-5}, f = 0.15$ and $R = 5000$. On top the absolute velocities of fluid and particles are displayed. On the bottom figures the velocity vectors of the fluid (a) or the u-velocity contours are given (b). Initial condition consists of streamwise vortices of the fluid (a), while the disturbance velocity of the particles is zero. For the response (b), low- and high-speed streaks can be clearly recognized.

height. The particles have no initial disturbance velocity. The perturbation at the final time is composed mainly of streamwise velocity, with two streaks antisymmetric with respect to the centerline, for both the fluid and particles. The lift-up effect is clearly at work also in particle-laden flows. Note that the particle velocity adjusts to the fluid velocity, although only the response of the fluid perturbation is considered. These equal velocities reduce the dissipation of energy due to fluid/particle interaction.

We now investigate the effect of S and f. In figure 9(a) the optimal growth is given for five different cases and a value of $S = 2.5 \cdot 10^{-3}$, larger than that in figure 7. The difference between the single phase flow and the case $fluid \rightarrow fluid$ is small, although present. It is interesting to note that, at this value of S, very large variations in the asymptotic stability of the two-phase flow are already observed, see figure 3. The presence of particles has therefore a completely different impact on modal and non-modal stability.

While the maximum gain of the fluid kinetic energy is hardly affected by the particles, the time at which the optimal growth is reached varies. To document this, the optimal growth is displayed as a function of time for $(\alpha, \beta) = (0, 2)$ and $R = 2000$ in figure 9(b) for $fluid \rightarrow fluid$. Here results for two values of f and two values of S are compared to the case without particles. The results indicate that the delay induced by the particles increases with increasing f, but that this delay is not affected by the value of S.

Figure 10 shows the optimal growth and the time to reach the optimal growth as a function of mass fraction f using $S = 2.5 \cdot 10^{-3}$ and $R = 2000$. The optimal growth increases by a

factor $(1+f)^2$ for the case $all \rightarrow all$ compared to the single phase flow, while for the cases $all \rightarrow fluid$ and $fluid \rightarrow all$ the optimal growth is enhanced only with a factor $(1+f)$. The time needed to reach the optimal growth on the other hand increases by $(1+f)$ for all cases, figure 10(b).

Two competing mechanisms appear to be present in this case. Losses are induced by the initial difference between fluid and particle velocity. These are proportional to the mass fraction f and cause a slower initial growth of the perturbation (figure 9b). Losses decrease faster for lower S, indicating shorter relaxation time, but this effect appears negligible. At the same time, once particles move at the fluid velocity, larger amplifications are observed (see $all \rightarrow fluid$ in figure 7 and figure 10). In conclusion, the amplification of the fluid kinetic energy in the presence of particles is slower because of the losses due to the initial difference between fluid and particle velocity but the potential growth is larger. *These two effects compensate and the total energy gain is similar in laden and unladen flow.*

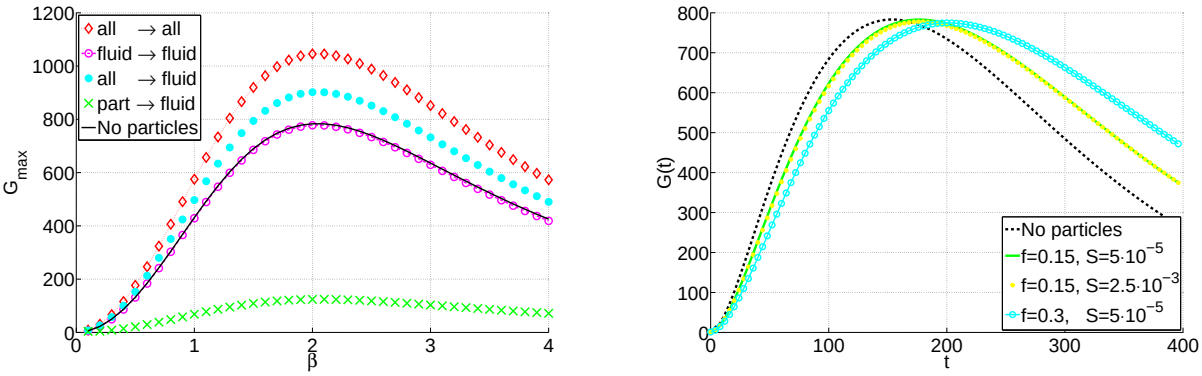

(a) Optimal growth

(b) Transient growth

Figure 9: (Color online) (a): Optimal growth for 5 different cases, including the clean fluid flow, using $\alpha = 0$, $f = 0.15$, $S = 2.5 \cdot 10^{-3}$ and $R = 2000$. (b): Transient growth for the case $fluid \rightarrow fluid$ with $\beta = 2$, $\alpha = 0$ and $R = 2000$, using $f = 0.3$ and 0.15 as well as $S = 2.5 \cdot 10^{-3}$ and $5 \cdot 10^{-5}$.

The optimal growth versus Reynolds number is given for spanwise perturbations in figure 11(a). The growth for spanwise waves is found to be proportional to R^2, as in the case of flows without particles. The results also confirm that non-modal growth is enhanced in the presence of particles, and, as shown by the inset in the figure, the energy gain for the case $all \rightarrow all$ is $(1+f)^2$ times that for the single phase flow. The transient growth appears to be proportional to the effective Reynolds number based on the total density of the medium $\rho_t = (1+f)\,\rho_{fluid}$ as in the case of modal stability at low values of S. In this case, however, the effect is observed also at large values of S. This again suggests that a different definition of the Stokes number may be more relevant for stability problems. We

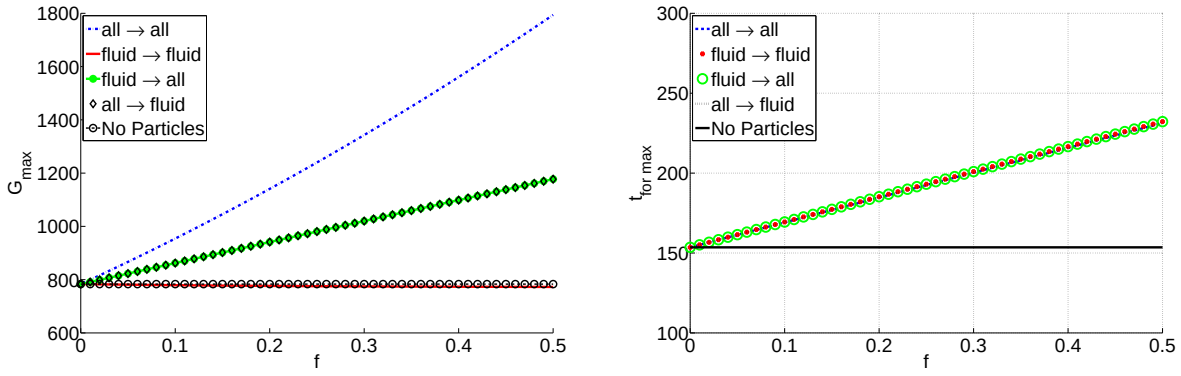

(a) $G_{max}(f)$ (b) $t_{for\ max}(f)$

Figure 10: (Color online) (a): G_{max} as a function of mass fraction f for several cases denoted in the legend using $S = 2.5 \cdot 10^{-3}$ and $R = 2000$. (b): $t_{for\ max}$ as a function of mass fraction f for the same cases as (a) using $S = 2.5 \cdot 10^{-3}$ and $R = 2000$.

therefore consider again the stability Stokes number St_ω, introduced above as the ratio of the particle relaxation time and the instability time scale. This parameter St_ω assumes low values for non-modal growth since the latter is occurring on a time scale longer than the characteristic particle relaxation time. The effect of particles on modal and non-modal stability can therefore be explained by this new parameter: at low values of St_ω, the solid phase acts only to increase the total density and therefore the effective Reynolds number. Significant energy losses having a stabilizing effect are found only when $St_\omega \approx 1$.

The optimal growth as a function of S is displayed in figure 11(b). The figure shows the flow behavior in the ballistic limit, when particles are not affected by the fluid, and quantifies when these effects become relevant. As shown by equations (5-8), for large SR the motion of fluid and particles are decoupled. Particles behave as the fluid but the particle velocity field is not required to be divergence free and there is no dissipation. In absence of dissipation, we observe that the particle perturbation velocity can grow significantly. This observation is in line width the inviscid algebraic instability first examined in Ref. 18 for streamwise-independent modes The same behavior is observed also for streamwise-dependent modes: here it can be seen as the inviscid Orr mechanism. The computations become grid-dependent and the optimal initial conditions for the particle velocity become as narrow as possible in the wall-normal direction, limited to non-zero values in the grid point associated to highest shear of the base flow. This is allowed since the velocity field for the particles does not need to be solenoidal and is in agreement with the inviscid limit of the Orr-Sommerfeld equation. Note however that the validity of our model is questionable for large particles, i.e. large S.

The case $fluid \rightarrow fluid$ does not show increased growth at large S, which indicates that indeed the large growth in the case $all \rightarrow all$ is associated to the energy of the particles. The

value of S does not have a very large effect on the optimal gain: the optimal growth between $S = 1 \cdot 10^{-5}$ and $S = 1 \cdot 10^{-2}$ is hardly changing. This confirms that particle relaxation time has little effect on non-modal stability since St_ω is low in the range considered; the main effect is from the mass fraction f that increases the fluid density.

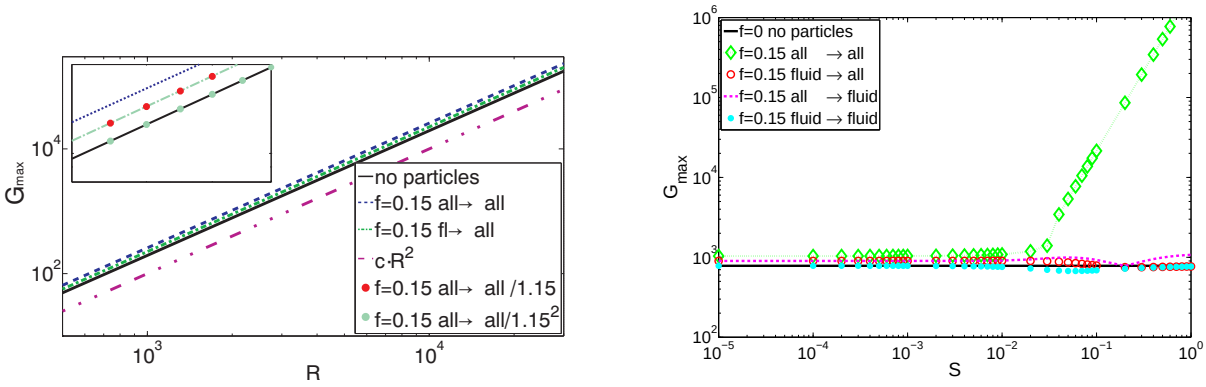

(a) $\beta = 2, \alpha = 0, S = 5 \cdot 10^{-5}$

(b) $\beta = 2, \alpha = 0, R = 2000$

Figure 11: (Color online) (a): optimal growth versus Reynolds number. In the large figure the cases for a clean fluid, the $all \rightarrow all$ and $fl \rightarrow all$ are given, in which the dependence of R^2 can be clearly recognized. As reference, a function of a constant times R^2 has been given as well, the blue line. In the insert the $all \rightarrow all$-case has been given, but then divided by $(1 + f)$(•) and $(1 + f)^2$(•). (b): the optimal growth versus S is displayed, for the same cases as in the left figure including $fluid \rightarrow fluid$.

2. Two-dimensional streamwise-dependent waves

The results for streamwise-dependent disturbances are first discussed referring to the results shown in figure 7(c-d). The energy gain for the case $all \rightarrow all$ is responsible for the largest possible energy gain, as for spanwise disturbances. For streamwise disturbances the increase with respect to the case of single phase flow is$(1 + f)$ for small values of S. For the cases where the initial condition consists of fluid velocity only, $fluid \rightarrow all$, its response in energy growth is less compared to the clean fluid flow. When only the particles are disturbed, $part \rightarrow all$, the response is even less at these low values of the particle relaxation time.

Investigating the response of the particles reflects the ability to produce mixing. The possible energy growth of the particles is small; all cases $initial \rightarrow part$ are small compared to the cases just presented. As already discussed for spanwise disturbances, this difference is of order f^{-1}. Furthermore, for $part \rightarrow part$ the maximum gain is always equal to one, i.e. no growth.

The final three cases discussed deal with the optimal energy growth of the fluid. The fluid gains less energy compared to the single phase flow. Even for a disturbance of the total system, $all \rightarrow fluid$, the energy gain is less compared to the single phase flow. The case $fluid \rightarrow fluid$ shows a decrease of the transient growth by more than a factor of $(1 + f)$. This indicates that for streamwise disturbances the particles introduce extra dissipation of the disturbance energy. An initial disturbance of the particles results in a small response to the fluid, $part \rightarrow fluid$, which again can be explained by the relative low density of the particles.

The initial condition and optimal response for a streamwise disturbance with $\alpha = 1.6, S = 5 \cdot 10^{-5}, f = 0.15$ and $R = 5000$ for the case $fluid \rightarrow fluid$ is displayed in figure 12. The initial condition consists of flow patterns opposing the mean shear direction. As time evolves, they tilt into the mean shear direction, which introduces the transient growth. This process is similar to the Orr-mechanism in fluid alone[27]. Note that at the final optimization time, the fluid and particle velocities are not exactly equal to each other, unlike for spanwise disturbances at the same value of S.

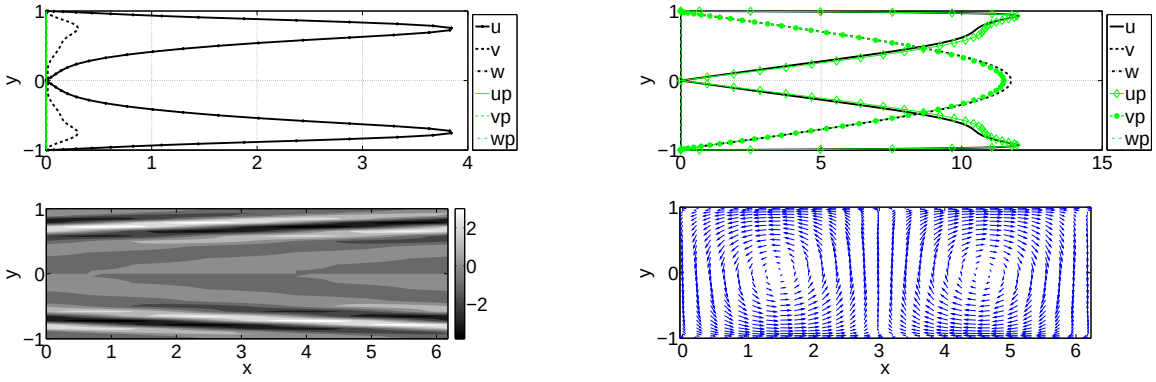

(a) Initial condition

(b) Response

Figure 12: (Color online) Optimal initial condition and response for the case $fluid \rightarrow fluid$ with $\alpha = 1.6, S = 5 \cdot 10^{-5}, f = 0.15$ and $R = 5000$. On top the absolute velocities of fluid and particles are displayed. The bottom figures represent the u-velocity contours (a) and the velocity vectors of the fluid (b). Initial condition can be seen as flow patterns opposing the mean shear (a). The disturbance velocity of the particles is zero. In the response (b), the disturbance is changed into the the mean shear direction. The Orr-mechanism can be recognized.

In figure 13(a) the optimal growth as function of α is displayed for particles with $S = 2.5 \cdot 10^{-3}$, a value larger than that used in figure 7. One notices a growth larger than in single phase fluid in three different cases, namely $all \rightarrow all$, $all \rightarrow fluid$ and $part \rightarrow fluid$. In other words, in all the cases with large energy growth, the initial condition consists of

particle disturbance velocity. This can be either as particles alone or as the total system, which includes particle velocity.

To investigate the effect of S on the growth of two-dimensional disturbances, figure 13(b) shows the optimal growth as a function of S. For small values of S, the results are as in figure 7(c). The energy gain is enhanced by a factor $(1+f)$ in the case $all \rightarrow all$ with respect to the single phase flow, unlike spanwise disturbances where the growth in the laden flow is enhanced by a factor $(1+f)^2$. When considering an initial disturbance consisting only of fluid velocity, $fluid \rightarrow fluid$ and $fluid \rightarrow all$, the energy gain is always smaller in the presence of particles. The particles induce therefore an energy loss. For the case of perturbation induced by the particle motion, $part \rightarrow fluid$, one observes that for values of $SR = \mathcal{O}(1)$ the transient growth increases significantly and reaches asymptotic values for the largest S considered. Larger values of the energy gain in the case of two-dimensional disturbances can therefore be observed when the particle relaxation time is longer than the typical convective time scale of the flow. Comparing the amplification with the case $all \rightarrow all$, one can see that this effect is associated to the growth of the particle perturbation kinetic energy in the ballistic limit. This was discussed before for spanwise-periodic modes.

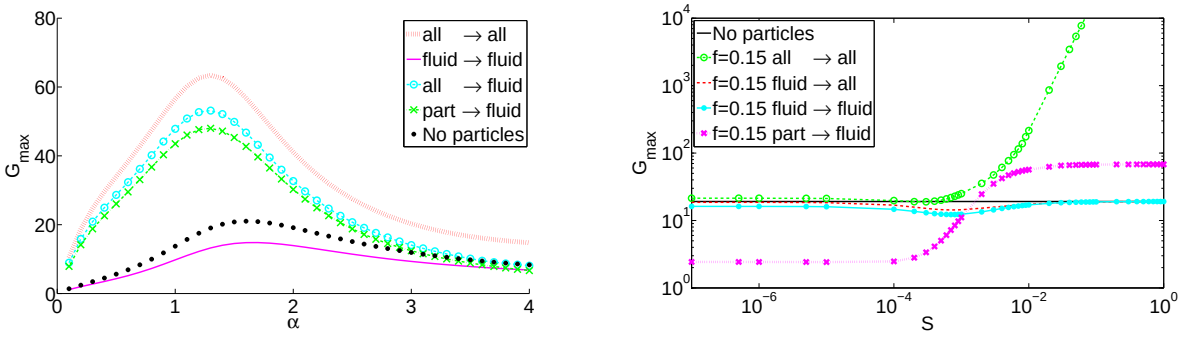

(a) $\beta = 0, S = 2.5 \cdot 10^{-3}$ and $R = 2000$

(b) $\beta = 0, \alpha = 2$ and $R = 2000$

Figure 13: (Color online) (a): optimal growth for streamwise waves for 5 different cases, including the single phase flow. (b): optimal growth versus S, for same cases as in the figure on the left. Note that $all \rightarrow all$ diverges from the other results at $S \sim 10^{-3}$

IV. CONCLUSIONS

We perform modal and non-modal stability analysis of channel flow seeded with small, heavy, spherical particles. The interaction between the two phases is modeled solely by Stokes drag. We present results for different values of the particle relaxation time and volume fraction. The particle relaxation time is limited by the fact that particle are assumed to be much smaller than the flow length scale, while the mass fraction is assumed small since

particle-particle collisions are not included in our model.

We show that the presence of particles has a very different effect on the exponential and transient growth of external perturbations. The differences are explained in terms of the different characteristic time scale of the two instability mechanisms. As shown in previous investigations, particles can increase the critical Reynolds number by at least one order of magnitude. However, we demonstrate here that particles increase the non-modal energy growth. The presence of a dilute solid phase therefore will not work as a flow-control strategy for maintaining laminar flow.

Modal stability is influenced by the dimensionless relaxation time, S. At small values (small particles) the critical Reynolds number decreases proportionally to the density of the solution, as $(1+f)$. Intermediate values of S yield the largest increase of the critical Reynolds number, where the increase is proportional to the volume fraction of the solid phase. In the ballistic limit, the neutral curves approach again the results for. The largest stabilization is obtained for $St_\omega = SR\omega_r \approx 1$, that is for waves whose period of pulsation is of the order of the particle relaxation time. To gain further insight into the stabilizing mechanisms we consider the evolution of the disturbance kinetic energy and show that the resonance between particle and instability characteristic times gives the maximum dissipation associated to the work of Stokes' drag.

The generation of streamwise streaks via the lift-up mechanism is still the dominant disturbance-growth mechanism in subcritical particle laden flows: the length scales of the most dangerous disturbances are unaffected while the disturbance growth can be initially delayed. The increase by a factor $(1+f)^2$ of the non-modal gain can also be explained in terms of the stability Stokes number St_ω. This dimensionless parameter assumes very low values in the case of the low-frequency non-modal growth ($St_\omega \approx SR/t_{max}$, with $t_{max} \approx \mathcal{O}(100)$) and therefore the effect of particles is just that of altering the fluid density. Particles have the time necessary to follow the slow formation of the streaks. Indeed particles increase the solution density and the Reynolds number of the laden fluid becomes then $R_m = (1+f)\,R$. As the optimal growth in unladen flows is proportional to R^2, the presence of the particles increases the energy gain by $(1+f)^2$.

To summarize, the effect of particles on the modal and non-modal stability of channel flows can be explained by the stability Stokes number St_ω. Low values of this parameter indicate that the particles follow passively the fluid instability and their effect is only that of increasing the total density of the suspension. Significant energy losses that can have a stabilizing effect are observed only when $St_\omega = \mathcal{O}(1)$.

A method for investigating the response of different flow quantities to different input disturbances has been introduced. Instead of optimizing the energy of the total system, we optimize for fluid and particles separately as well. When examining a disturbance in the fluid alone and the corresponding fluid energy at final time, we find that the optimal growth for a particle laden flow is close to that of the clean fluid and a noticeable difference is seen only for the largest values of S. The energy that the fluid can extract by an initial

perturbation of the particle velocity is proportional to the mass fraction f.

The work presented in this paper could be extended in a number of non-trivial and interesting ways. First, we have here focussed on heavy particles, neglecting contributions from added mass and pressure forces. The effect of light particles on the flow stability should be addressed. Second, one may consider finite-size particles of different shapes. Finally, our results indicate that the initial stages of transition in dilute suspensions of small particles should follow a similar path as in a single phase flow. However, to be able to estimate the effect of the solid phase on the laminar/turbulent transition full nonlinear simulations will be necessary. Indeed, while little changing the initial formation of the streamwise elongated streaks, particles may accumulate and affect the self-sustaining cycle of turbulence[33]. The recent results in turbulent channel flow[2] indicate that this may be the case.

---

[1] W. T. Sproull. Viscosity of Dusty Gases. *Nature*, 190:976–978, June 1961.

[2] L. H. Zhao, H. I. Andersson, and J. J. J. Gillissen. turbulence modulation and drag reduction by spherical particles. *Phys. Fluids*, 22:081702, 2010.

[3] P. G. Saffman. On the stability of laminar flow of a dusty gas. *J. Fluid Mech.*, 13:120–128, 1962.

[4] D. H. Michael. The stability of plane Poiseuille flow of a dusty gas. *J. Fluid Mech.*, 18:19–32, 1964.

[5] V.Ya. Rudyak, E.B. Isakov, and E.G. Bord. Hydrodynamic stability of the poiseuille flow of dispersed fluid. *J. Aerosol Sc.*, 82:53–66, 1997.

[6] E. S. Asmolov and S. V. Manuilovich. Stability of a dusty-gas laminar boundary layer on a flat plate. *J. Fluid Mech.*, 365:137–170, June 1998.

[7] E. Calzavarini, R. Volk, M. Bourgoin, E. Lévêque, J.-F. Pinton, and F. Toschi. Acceleration statistics of finite-sized particles in turbulent flow: the role of Faxén forces. *J. Fluid Mech.*, 630:179–189, June 2009.

[8] M. R. Maxey and J. J. Riley. Equation of motion for a small rigid sphere in a nonuniform flow. *Phys. Fluids*, 26:883–889, April 1983.

[9] C. M. Tchen. *Mean value and correlation problems connected with the motion of small particles suspended in a turbulent fluid*. PhD thesis, Delft, 1947.

[10] S. Corrsin and J. Lumley. On the equation of motion for a particle in turbulent fluid. *Appl. Sci. Res.*, A6:114–116, 1956.

[11] S. A. Boronin and A. N. Osiptsov. Stability of a Disperse-Mixture Flow in a Boundary Layer. *Fluid Dynamics*, 43:66–76, February 2008.

[12] P. G. Saffman. The lift on a small sphere in a slow shear flow. *J. Fluid Mech.*, 22:385–400, June 1965.

[13] D. S. Dandy and H. A. Dwyer. A sphere in shear flow at finite reynolds number: effect of shear

on particle lift, drag, and heat transfer. *J. Fluid Mech.*, 216:381–400, 1990.

[14] R. Mei. An approximate expression for the shear lift force on a spherical particle at finite reynolds number. *Int. J. Multiphase Flow*, 18:145–147, 1992.

[15] J. B. McLaughlin. Inertial migration of a small sphere in linear shear flows. *J. Fluid Mech.*, 224:262–274, 1991.

[16] A. W. Vreman. Macroscopic theory of multicomponent flows: Irreversibility and well-posed equations. *Physica D*, 225:94–111, 2007.

[17] S. A. Boronin. Investigation of the stability of a plane-channel suspension flow with account for finite particle volume fraction . *Fluid Dynamics*, 43:873–884, December 2008.

[18] T. Ellingsen and E. Palm. Stability of linear flow. *Phys. Fluids*, 18:487–488, 1975.

[19] L. N. Trefethen, A. E. Trefethen, S. C. Reddy, and T. A. Driscoll. Hydrodynamic stability without eigenvalues. *Science*, 261:578–584, 1993.

[20] S. C. Reddy and D. S. Henningson. Energy growth in viscous channel flows. *J. Fluid Mech.*, 252:209–238, 1993.

[21] P. J. Schmid and D. S. Henningson. *Stability and transition in shear flows*. Springer, 2001.

[22] M. T. Landahl. A note on an algebraic instability of inviscid parallel shear flows. *J. Fluid Mech.*, 98, part 2:243–251, 1980.

[23] S. C. Reddy, P. J. Schmid, J. S. Baggett, and D. S. Henningson. On the stability of streamwise streaks and transition thresholds in plane channel flows. *J. Fluid Mech.*, 365:269–303, 1998.

[24] P. A. Elofsson, M. Kawakami, and P. H. Alfredsson. Experiments on the stability of streamwise streaks in plane Poiseuille flow. *Phys. Fluids*, 11:915–930, 1999.

[25] L. Brandt and D. S. Henningson. Transition of streamwise streaks in zero-pressure-gradient boundary layers. *J. Fluid Mech.*, 472:229–261, 2002.

[26] G. Boffetta, A. Celani, F. De Lillo, and S. Musacchio. The Eulerian description of dilute collisionless suspension. *EPL (Europhysics Letters)*, 78:14001, 2007.

[27] W. M. F. Orr. The stability or instability of the steady motions of a perfect liquid and of a viscous liquid. Part I: A perfect liquid. Part II: A viscous liquid. In *Proc. Roy. Irish Acad. A*, volume 27, pages 9–138, 1907.

[28] C. Cossu and L. Brandt. On Tollmien-Schlichting-like waves in streaky boundary layers. *Eur. J. Mech./B Fluids*, 23:815–833, 2004.

[29] B. F. Farrell. Optimal excitation of perturbation in viscous shear flow. *Phys. Fluids*, 32:2093–2102, 1988.

[30] K. M. Butler and B. F. Farrell. Three-dimensional optimal perturbations in viscous shear flow. *Phys. Fluids A*, 4:1637–1650, 1992.

[31] L. H. Gustavsson. Energy growth of three-dimenisonal disturbances in plane Poiseuille flow. *J. Fluid Mech.*, 224:241–260, 1991.

[32] D. S. Henningson, A. Lundbladh, and A. V. Johansson. A mechanism for bypass transition from localized disturbances in wall-bounded shear flows. *J. Fluid Mech.*, 250:169–207, 1993.

[33] F. Waleffe. Hydrodynamic stability and turbulence: Beyond transients to a self-sustaining process. *Stud. Appl. Math.*, 95:319–343, 1995.